

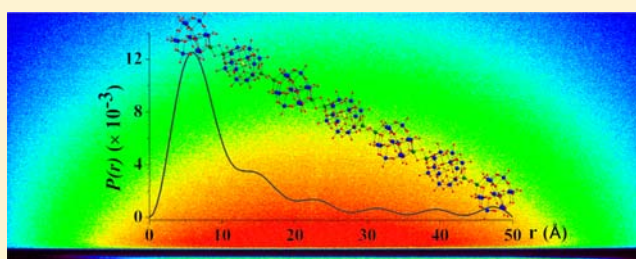
# Observing Assembly of Complex Inorganic Materials from Polyoxometalate Building Blocks

Yu Hou, Lev N. Zakharov, and May Nyman\*

Department of Chemistry and Center for Sustainable Materials Chemistry (CSMC), Oregon State University, Corvallis, Oregon 97331-4003, United States

**S** Supporting Information

**ABSTRACT:** Understanding the aqueous state of discrete metal-oxo clusters, prenucleation clusters, and even simple ions is valuable for controlling the growth of metal-oxide materials from water. Niobium polyoxometalates (Nb-POMs) are unique in the aqueous metal-oxo cluster landscape in their unusual solubility behavior: specifically, their solubility in water increases with increasing ion-pairing contact with their counterions, and thus provides a rare opportunity to observe these and related solution phenomena. Here, we isolate in the solid state the monomeric and dimeric building blocks, capped Keggin ions, of the extended Keggin chain materials that are now well-known: not only in Nb-POM chemistry, but Mo and V POM chemistry as well.  $\text{Rb}_{13}[\text{GeNb}_{13}\text{O}_{41}] \cdot 23\text{H}_2\text{O}$  (**Rb1**),  $\text{Cs}_{10.6}[\text{H}_{2.4}\text{GeNb}_{13}\text{O}_{41}] \cdot 27\text{H}_2\text{O}$  (**Cs1**) and  $\text{Cs}_{18}\text{H}_6[(\text{NbOH})\text{-SiNb}_{12}\text{O}_{40}]_2 \cdot 38\text{H}_2\text{O}$  (**Cs2**) were characterized by single-crystal X-ray diffraction. Small angle X-ray scattering (SAXS) of solutions of **Rb1** and **Cs1** in varying conditions revealed oligomerization of the monomers into chain structures: the extent of oligomerization is controlled by pH, concentration, and the counterion. We distinctly observe chains of up to six Keggin ions in solution, with the large alkali cations for charge-balance. This combined solid state and solution study reveals in great detail the growth of a complex material from discrete monomeric building blocks. The fundamentals of the processes we are able to directly observe in this study, ion-association and hydrolysis leading to condensation, universally control the self-assembly and precipitation of materials from water.



## INTRODUCTION

Inorganic nanoscale metal oxide clusters, especially but not limited to Group V and Group VI elements, resemble discrete units of a metal oxide lattice, both in form and in behavior. Thus they are valuable as both models and functional species in numerous applications including catalysis,<sup>1–3</sup> ion or electron mobility,<sup>4–8</sup> understanding aqueous interfaces of materials,<sup>9</sup> and as preassembled building blocks for both complex<sup>10–13</sup> and simple<sup>14–18</sup> material forms. Moreover, the ion-association, hydrolysis, and condensation reactions that lead to self-assembly of clusters into materials are at the heart of virtually all synthetic and natural aqueous inorganic processes.<sup>19–24</sup> Thus observing these processes directly in solution by methods such as small-angle X-ray scattering (SAXS) can provide valuable insight into fundamental aqueous ion behaviors that control crystallization, dissolution, transport, ion-exchange, and adsorption and desorption at interfaces. Yet the inorganic scientific community is only beginning to use this technique to full advantage.<sup>18,25–31</sup>

One general theme to assemble complex materials from metal-oxo clusters is to simply link them together with metal cations in mild aqueous conditions. This has been well-demonstrated with vanadium, tungsten, molybdenum, and niobium polyoxometalates (POMs; anionic metal oxo clusters of early  $d^0$  transition metals); the resulting materials have ion-

exchange,<sup>32–34</sup> luminescent,<sup>35–37</sup> and catalytic<sup>38,39</sup> functionalities. The chemistry of both the metal cations and the POMs can be tailored to favor linkage into 1, 2, or 3-dimensional materials. Large, high-coordinate metals such as rare-earths and some open-shell transition metals readily link together POMs through multidentate coordination with the POM oxo ligands.<sup>36–38</sup> Highly charged POMs, especially those of Group V and multielectron reduced clusters of Group VI, tend to bind charge-reducing cationic *metyl* ‘caps’ (i.e.,  $\text{Mo}=\text{O}^{4+}$ ,  $\text{V}=\text{O}^{3+}$ ,  $\text{Nb}=\text{O}^{3+}$ ,  $\text{Ti}=\text{O}^{2+}$ , etc.): with their tendency to dimerize, these *metyl* caps provide a second example of self-assembly of complex materials from cluster building-blocks.<sup>32–34,38–42</sup>

Prior work<sup>32–34,39–42</sup> on the development of POMs of Nb (Nb-POMs) has produced numerous examples of  $[\text{XNb}_{12}\text{O}_{40}]^{15/16-}$  ( $\text{X} = \text{Si}, \text{Ge}, \text{P}$ ) Keggin ions that are linked into 1 and 2-dimensional materials by  $[\text{Nb}_2\text{O}_2]^{6+}$  or  $[\text{Ti}_2\text{O}_2]^{4+}$  bridges; the different arrangements of these into lattices is illustrated in Figure 1. Recent work on Nb-POMs has revealed their unusual solubility trend with alkali counteranions: that is, highest solubility occurs with maximum ion-pairing between the anionic POMs and alkali cations.<sup>43–47</sup> Thus the Rb and Cs

Received: August 20, 2013

Published: October 11, 2013

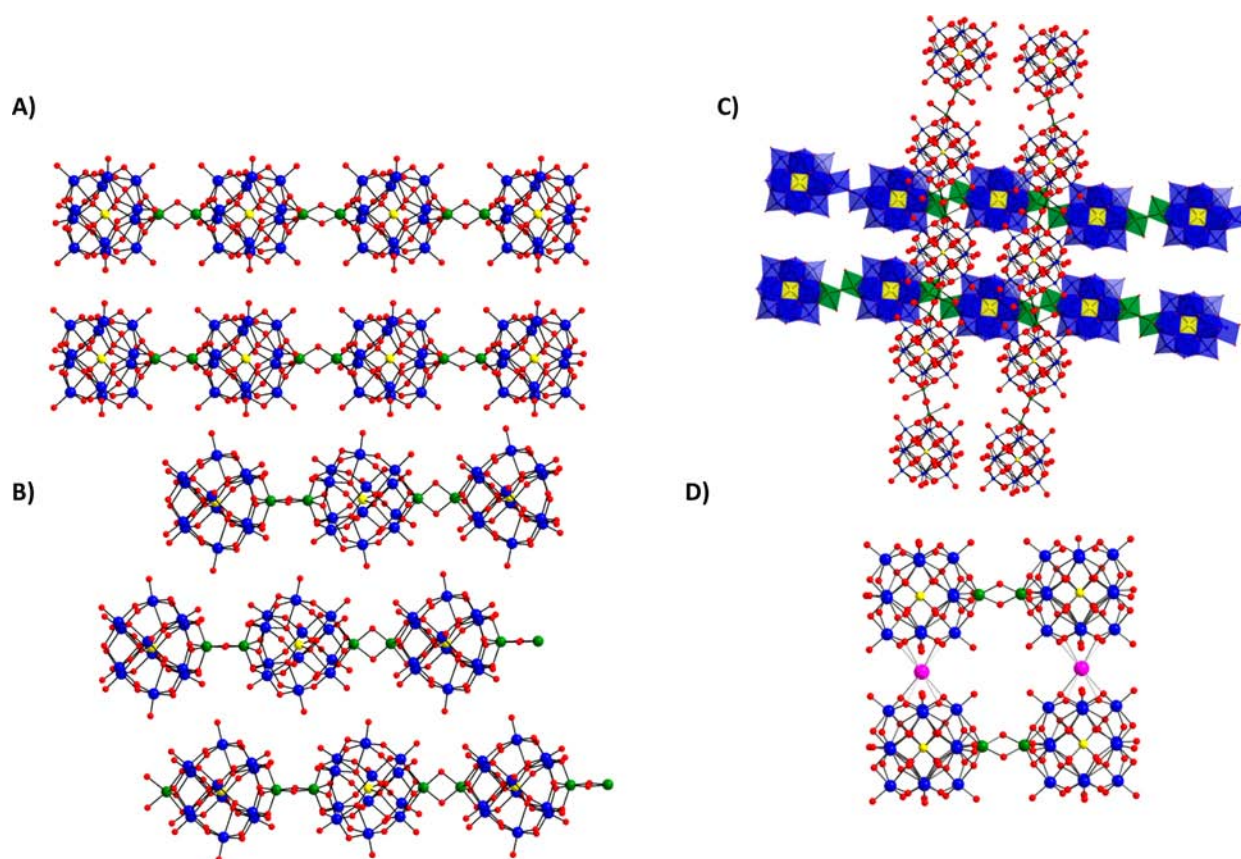


**Figure 1.** Illustrating linking dodecaniobate  $[\text{XNb}_{12}\text{O}_{40}]^{15/16-}$  ( $\text{X} = \text{Si}, \text{Ge}, \text{P}$ ; yellow spheres) Keggin ions into infinite lattices to form complex materials, as observed in the solid-state. Blue spheres or blue polyhedra are Keggin-ion Nb or  $\text{NbO}_6$ , respectively, green spheres or green polyhedra are linking Ti/Nb or  $[(\text{Ti},\text{Nb})_2\text{O}_2]$ , respectively. (A)  $[\text{XNb}_{12}\text{O}_{40}]^{15/16-}$  linked into parallel chains with Keggin ions of adjacent chains aligned.<sup>32</sup> (B)  $[\text{SiNb}_{12}\text{O}_{40}]^{16-}$  linked into chains with Keggin ions of adjacent chains offset.<sup>42</sup> (C) Chains aligned perpendicular to each other in alternating layers.<sup>39</sup> Back layer is shown in polyhedral representation for clarity of viewing. (D) Keggin ions linked into sheets, with bridging  $[\text{Nb}_2\text{O}_2]^{6+}$  in one direction and  $\text{K}^+$  (pink spheres) in the second direction.<sup>33</sup> These chains and layers are all anionic, and the charge-balancing  $\text{Na}^+$  and/or  $\text{K}^+$  counterions have been removed for ease of viewing.

salts of Nb-POMs are highly soluble, while the Li and Na salts are rather insoluble: this is opposite of the behavior of most cation–anion pairs. In the interest of furthering our understanding of the anomalous solubility trend of Nb-POMs, the self-assembly of Nb-POM materials, and the generalities of cation–anion association in water, we have isolated the capped Keggin-ion  $[\text{GeNb}_{12}\text{O}_{40}(\text{Nb}=\text{O})]^{13-}$ , the monomeric building block of low-dimensional materials comprising linked dodecaniobate Keggin ions. Not surprisingly, this anionic cluster is isolated as highly soluble Rb and Cs salts. Small-angle X-ray scattering (SAXS) clearly reveals spontaneous self-assembly of these monomeric building-blocks into linear chains, as well as the role of concentration, pH, and the counterions on the assembly process.

## RESULTS AND DISCUSSION

### Synthesis and Solid-State Structures of Rb1 and Cs1.

$\text{Rb}_{13}[\text{GeNb}_{13}\text{O}_{41}] \cdot 23\text{H}_2\text{O}$  (**Rb1**) and  $\text{Cs}_{10.6}[\text{H}_{2.4}\text{GeNb}_{13}\text{O}_{41}] \cdot 27\text{H}_2\text{O}$  (**Cs1**) were synthesized hydrothermally and crystallized by diffusion of methanol into the clear aqueous mother liquor solutions from the hydrothermal processing, similar to what has been described prior (see SI for further detail).<sup>44,45</sup> **Rb1** (CSD-426505) is of trigonal symmetry ( $P\bar{3}$ ) and **Cs1** (CSD-426588) is cubic ( $Fd\bar{3}m$ ). Both feature the anion  $[\text{GeNb}_{13}\text{O}_{41}]^{13-}$  (**1**) which can also be described as  $[\text{GeNb}_{12}\text{O}_{40}(\text{Nb}=\text{O})]^{13-}$ ; a

Keggin-ion with a single  $[\text{Nb}=\text{O}]^{3+}$  cap, and is illustrated in Figure 2. In both **Cs1** and **Rb1**, there is structural disorder in this capping position. For **Rb1**, there are three equivalent positions for the cap that are related by one of the  $C_3$  axes (parallel to a Ge–O bond) of the Keggin ion, and this

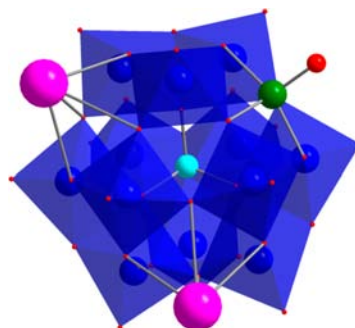


**Figure 2.** Illustrating the disorder of the **Rb1** anion,  $[\text{Rb}_2(\text{Nb}=\text{O})\text{GeNb}_{12}\text{O}_{40}]^{11-}$ . Turquoise sphere and blue polyhedra comprise the Ge and  $\text{NbO}_6$  of the core Keggin ion, respectively. 2/3rd of the disordered site is occupied by a  $\text{Rb}^+$  cation (pink spheres) with four bonds to Keggin ion oxo ligands. 1/3rd of the site is occupied by an  $\text{Nb}=\text{O}$  cap with four bonds to Keggin ion oxo ligands (green sphere is Nb, red sphere is the oxo-ligand). The pink spheres and red sphere occupy the same crystallographic site.

Table 1. Calculated Form Factor Parameters for Rb1 and Cs1 in TMAOH Solution

A <sup>+</sup>	concentration (mM)	R <sub>g</sub> (Guinier approximation) Å	spherical radius <sup>a</sup> Å	R <sub>g</sub> (from PDDF) <sup>b</sup> Å	maximum linear extent (from PDDF) <sup>b</sup> Å	χ <sup>2</sup> (PDDF)	solution pH
Rb	1.2	4.5 (1)	5.8	4.5 (2)	11.4 (2)	0.78	13.60
Rb	6.0	4.6 (1)	6.0	4.6 (1)	14.2 (2)	5.32	
Rb	12.0	4.6 (2)	5.9	4.9 (4)	15.3 (1)	5.59	
Rb	24.0	4.2 (1)	5.5	5.1 (1)	16.2 (2)	4.93	
Average		4.5 (1)	5.8				
Size parameters determined from crystal structure (Å)							
From center to cap/Rb: 5.7 (R <sub>g</sub> = 4.4) Diameter = 11.4				From center to extent of core Keggin: 5.4 (avg) (R <sub>g</sub> = 4.2) Diameter = 10.7			
Cs	1.0	4.6 (1)	5.7	4.5 (1)	12.6 (1)	2.77	13.72
Cs	6.0	4.7 (1)	6.0	4.8 (4)	14.5 (2)	1.95	
Cs	12.0	4.3 (1)	5.6	5.0 (3)	15.4 (1)	1.22	
Cs	24.0	4.3 (2)	5.5	5.1 (2)	16.1(6)	2.40	
Average		4.4 (2)	5.7				
Size parameters determined from crystal structure (Å)							
From center to cap/Cs: 5.8 (R <sub>g</sub> = 4.5) Diameter = 11.5				From center to extent of core Keggin: 5.4 (R <sub>g</sub> = 4.2) Diameter = 10.7			

<sup>a</sup>Calculated from R<sub>g</sub>. Radius ~ 1.29\*R<sub>g</sub> for spherical particle. <sup>b</sup>From the Moore function<sup>49</sup> in Irena PDDF analysis.

Table 2. Calculated Form Factor Parameters for Rb1 and Cs1 in Water

A <sup>+</sup>	concentration (mM)	R <sub>g</sub> (Guinier approximation) Å	R <sub>g</sub> (from PDDF) <sup>a</sup> Å	maximum linear extent; (from PDDF) Å	reduced χ <sup>2</sup>	solution pH
Rb	1.2	6.3(1)	11.4(1)	32.4(1)	1.80	9.60
Rb	2.4	6.4(1)	13.1(1)	41.0(1)	1.14	10.71
Rb	6.0	6.6(1)	9.6(1)	32.4(3)	2.89	10.73
Rb	12.0	6.5(1)	10.6(1)	51.3(5)	2.59	10.73
Rb	24.0	6.5(1)	10.8(1)	50.2(3)	1.32	11.00
Cs	1.2	5.1(1)	5.2(1)	15.0(1)	0.34	10.75
Cs	6.0	5.3(1)	5.3(1)	16.0(2)	1.11	10.74
Cs	12.3	5.3(1)	5.5(1)	17.2(1)	2.17	10.74
Cs	18.0	5.7(1)	5.8(1)	16.9(1)	2.56	10.73
Cs	24.6	5.4(2)	5.6(1)	16.6(1)	2.48	10.63

<sup>a</sup>Calculated from R<sub>g</sub>. Radius ~ 1.29\*R<sub>g</sub> for spherical particle. <sup>b</sup>From the Moore function<sup>49</sup> in Irena PDDF analysis.

symmetry-related site is 1/3rd occupied with Nb=O and 2/3rd occupied with Rb<sup>+</sup> in the O-position of the Nb=O unit. In Cs1, there are six of these positions related by a S<sub>6</sub> axis, which are 1/6th occupied with Nb=O, and 5/6th occupied with Cs<sup>+</sup>. Both Cs1 and Rb1 have one Nb=O per Keggin-ion. The Nb=O cap is a distorted square pyramid with two Nb–O bonds at ~2.1–2.2 Å (trans), two Nb–O bonds at ~1.8–1.9 Å, and the Nb=O bond distance of 1.75–1.76 Å (see Tables S1 and S2). The Rb–O<sub>Keggin</sub> and Cs–O<sub>Keggin</sub> bonds of this disordered site range from 2.9 to 3.1 Å in the solid-state. In the Rb1 lattice, there is a second disordered Rb-site that follows the Rb/Nb=O disorder. This Rb site is 1/3rd occupied: it is located 2.860(5) Å from the disordered Rb/oxo-cap site, and thus its occupancy is simultaneous with the adjacent Nb=O cap, and vacant when the Rb occupies the Keggin-capping site. The number of lattice water agrees with that found by thermogravimetry (see SI). All thirteen charge-balancing cations were located in the lattice, with an R-value for refinement of 4.89%. In Cs1, in addition to the five Cs<sup>+</sup>-cations disordered with the cap, the Keggin-ions are further capped by four Cs<sup>+</sup> arranged tetrahedrally around the Keggin ion, and these bridge to a second cluster, forming a supertetrahedral network of Keggin ions linked by cesium cations, with a total of seven charge-balancing Cs-cations per cluster. Approximately 3.6 more Cs<sup>+</sup>-cations were located, disordered with water molecules in the lattice space formed by this supertetrahedral network of cluster anions and linking Cs<sup>+</sup>-cations. Cs-H<sub>2</sub>O occupancy was optimized manually, based on

intersite distances, thermal parameters, charge-balance requirements, and thermogravimetry. It is interesting to note here that only the Ge-heteroatom consistently gave the capped form of the dodecaniobate Keggin ion. The Si-heteroatom, on the other hand, more readily templates [SiNb<sub>18</sub>O<sub>54</sub>]<sup>14-</sup> or [SiNb<sub>12</sub>O<sub>40</sub>]<sup>16-,45</sup>, and Ga and Al also give the octadecamer.<sup>44</sup>

**SAXS Analysis of Rb1 and Cs1 in Solution.** We prepared solutions of Rb1 and Cs1 ranging from 1 to 24 mmol concentration of the cluster, in both water and 0.278 molar TMAOH (tetramethylammonium hydroxide) solution. Concentrations for analysis were limited by scattering intensity at low concentrations and poorer solubility at high concentrations. The strategy of utilizing a TMAOH electrolyte solution was to provide conditions in which the clusters would not readily protonate and aggregate, as we presume these alkaline POMs have a tendency to do in neat water.<sup>48</sup> Thus TMAOH solutions served as a control to observe the clusters in their monomeric form. These data are summarized in Tables 1 (TMAOH solutions) and 2 (aqueous solutions with no electrolyte added).

**Rb1 and Cs1 in TMAOH Solution.** Table 1 summarizes pertinent form factor parameters of Rb1 and Cs1 in solutions of TMAOH. By using the Guinier approximation in the low-*q* (nm<sup>-1</sup>) region of the scattering curve (slope of *q*<sup>2</sup> vs ln(Intensity)), the radius of gyration (R<sub>g</sub>) of the approximately spherical scatterers was determined across the range of concentrations (see Table 1). The R<sub>g</sub> for Cs1 and Rb1 is consistent over 4 concentrations (2 orders of magnitude) with an averaged value of 4.5 Å for Rb1 and 4.4 Å for Cs1. The R<sub>g</sub>

estimated from the spherical radius ( $R_s \sim 1.29R_g$ ) derived from X-ray data for (1) a capped/alkali associated Keggin ion and (2) a 'nude' Keggin ion are (1) 4.42 Å for the Rb1 and 4.47 Å for Cs1, and (2) 4.16 Å for the 'nude' Keggin ion. The experimental  $R_g$  values of Rb1 and Cs1 dissolved in TMAOH solution are clearly very close to that which we expect for the capped/alkali-associated cluster. The pair distance distribution functions (PDDF), probability ( $p(r)$ ) as a function of radial distance from the edge of the particle ( $r = 0$ ), were determined for all solutions using the Moore function<sup>49</sup> in Irena<sup>50</sup> (see Tables 1 and 2). In this curve-fitting analysis that includes most of the measured  $q$ -range, the  $R_g$  values are similar to those obtained by the Guinier approximation for the more dilute solutions, suggesting these dilute solutions in TMAOH are monodisperse; see Figure 3. For both Rb1 and Cs1, the Moore

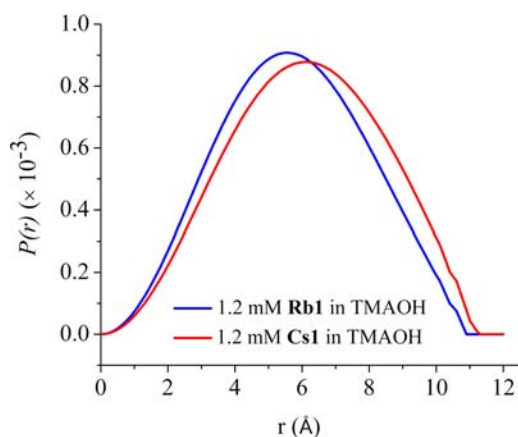


**Figure 3.** PDDF (pair distance distribution function), probability  $P(r)$  vs radius ( $r$ ) of the lowest concentration of Rb1 and Cs1 in TMAOH solution, exhibiting monodispersity under these conditions.

analysis suggests the  $R_g$  and the linear extent increase as a function of concentration, with formation of a second peak; see SI. This indicates either increasing alkali–cluster association or increasing cluster–cluster association. By approximating the two peak positions by fitting with Gaussian curves, we determined the peak maximum of the second peak is always double that of the first. This suggests that in TMAOH solution, with increasing concentration, Rb1 and Cs1 undergo some dimerization. This will be discussed in greater detail below, with regard to the behavior of Rb1 and Cs1 in water.

These data also indicate that in these high pH TMAOH solutions (>13, see Table 1) the cap remains intact, unlike the V=O capped dodecaniobate Keggin ions reported previously which dissociate their cap at higher pH.<sup>51,52</sup> Electrospray ionization mass spectrometry (ESI MS) also provided evidence for the cap remaining intact in solution. By ESI MS analysis, we found that the  $\text{GeNb}_{13}$  polyanion and its fragments with associated  $\text{Cs}^+$ ,  $\text{Rb}^+$ , and  $\text{H}^+$  ions with  $-3$ ,  $-4$ , and  $-5$  charge states are present in the dilute ( $10^{-6}$  molar) aqueous solutions (see SI).

Raman spectroscopy, along with SAXS and ESI MS provided a third mechanism to compare solid and solution states of Rb1 and Cs1. The Raman spectra of Rb1 and Cs1 as a solid, a TMAOH solution, and dissolved in neat water are shown in Figure 4. There are three major general frequency ranges identified<sup>53</sup> for the Nb–O bonds of the core Keggin: these are illustrated in Figure 4 and include (1) Nb–O<sub>c</sub> ( $150\text{--}300\text{ cm}^{-1}$ ), (2) Nb–O<sub>b</sub>–Nb ( $400\text{--}550\text{ cm}^{-1}$ ), and (3) Nb=O<sub>t</sub> ( $800\text{--}900\text{ cm}^{-1}$ ). By comparing Raman spectra of Rb1 and Cs1 to that of a Na-salt of  $[\text{GeNb}_{12}\text{O}_{40}]^{16-}$  (an uncapped Keggin ion) we hypothesize identification of four small but distinct peaks at  $\sim 790$ ,  $700$ ,  $385$ , and  $350\text{ cm}^{-1}$ . All of these peaks except  $350\text{ cm}^{-1}$  are present in the spectrum of the Keggin-ion that does not have a cap. Therefore  $350\text{ cm}^{-1}$  is identified as the  $2.1\text{--}2.2\text{ Å}$  Nb–O<sub>b</sub> bond of the cap, in accordance with an empirical correlation of Nb–O bond lengths to Raman peak positions.<sup>54</sup> We presume the vibrational bands of the Nb–O<sub>b</sub> bonds at  $\sim 1.8\text{--}1.9\text{ Å}$  and the Nb=O<sub>t</sub> bond of the cap overlap with the large vibrational bands of the core Keggin ion. The vibrational frequencies at  $790$ ,  $700$ , and  $385\text{ cm}^{-1}$  are assigned to the  $\text{GeO}_4$  central anion. Only the Nb=O<sub>t</sub> bond has significant sharpness so that we can accurately observe its shifts upon dissolution. This peak for both Rb1 and Cs1 is located at  $876\text{ cm}^{-1}$ . Dissolved in TMAOH solution, this peak does not shift for either salt. However, upon dissolution in water for both Rb1 and Cs1, there is a discernible shift to  $885\text{ cm}^{-1}$ . Computational studies predicting vibrational frequencies (infrared and Raman) in a vacuum and in solvent suggest an increase in bond length and corresponding decrease in vibrational frequency for these types of metal–oxygen vibrations in polyoxometalates.<sup>55</sup> This is due to increased interactions of these oxo ligands with water molecules via H-bonding. The Raman analysis of Rb1 and Cs1 suggests that while bonding/interactions of the cluster anion with counterions and water are similar between the solid-state

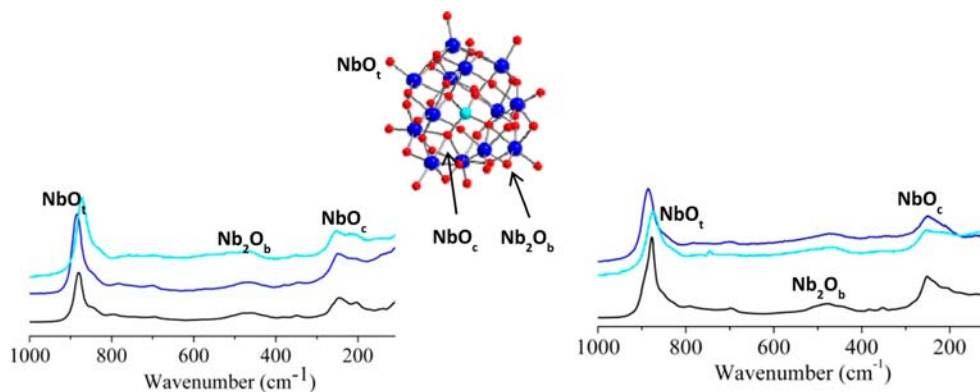


**Figure 4.** Raman spectra of Cs1 (left) and Rb1 (right) as a solid (black), in water (blue), and in TMAOH (torquoise), showing the peak shift of the  $\nu$ -oxygen bonded to Nb (Nb–O<sub>c</sub>) upon dissolution in water.

and TMAOH solutions, these interactions actually decrease in water. This is probably due to the various aggregation processes that we observe via SAXS, discussed below.

**Rb1 and Cs1 in Water.** The scattering curves for these solutions are much more complex, and thus we approach the analysis with some caveats! However, it is very clear that **Rb1** undergoes extensive chain-oligomerization in neat water, which increases with concentration (see Figure 5), as will be discussed

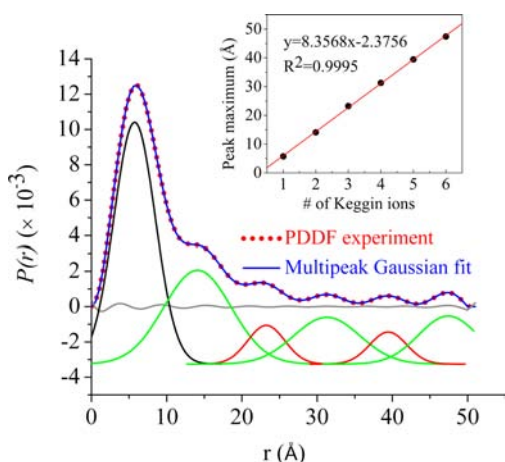


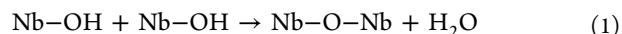
**Figure 5.** Fit of the PDDF analysis of 24 mmolar **Rb1** in water. The black fitted peak is the monomer, and the short axis of the oligomers. Green fitted peaks are the long axes of chains containing an even number of Keggin ions (dimer, tetramer, and hexamer). Red fitted peaks are the long axes of chains containing odd numbers of Keggin ions (trimer, pentamer). Gray is the difference of the experimental data and the multipeak Gaussian fit. Inset: plot of fitted peak maxima (Å) vs number of Keggin ions in the chain.

later. The  $R_g$  values obtained from the Guinier region of the scattering curves are considerably larger than those of the TMAOH solutions: around 6.5 Å for **Rb1** and ~5.5 Å for **Cs1** (Table 2), which is our first indication that these solutions are unlike the TMAOH solutions. The  $R_g$  values from the PDDF analyses are slightly larger than those obtained from the Guinier approximation for **Cs1**, with the maximum linear extent ranging from 15 to 17 Å. This is not too dissimilar from the higher concentration **Cs1** solutions in TMAOH.

The  $R_g$  values from the PDDF analysis for **Rb1** in water range from ~9 to 13 Å, considerably larger than those determined from the Guinier analysis, and certainly much larger than those of equivalent solutions of **Cs1**. Furthermore, the linear extents are up to 50 Å! The shapes of  $p(r)$  curves strongly suggest chain oligomerization, as illustrated in solid-state structures shown in Figure 1. The lowest concentration, 1.2 mmolar **Rb1**, shows that monomers, dimers, and trimers are present; 2.4 and 6 mmolar **Rb1** in water contain up to four Keggin ions linked together, and the 12 and 24 mmolar solutions have as many as six Keggin ions linked into still-soluble chains (see Figure S3).

The pH values of analyte solutions, listed in Table 2, are of interest in considering both linkage and aggregation processes. At lowest concentrations of **Rb1** and **Cs1** in water, **Cs1** has a higher pH, and it is fairly consistent with increasing concentration. **Rb1** on the other hand increases from 9.6 to 11 with increasing concentration. The increase in pH is due to the well-known protonation of cluster oxygens by the very basic, highly charged Nb-POMs.<sup>46</sup> We attribute the lack of

increase of pH with increasing **Cs1** concentration to more ion-contact association with Cs compared to Rb, as discussed previously. This phenomenon may both block sites for protonation on the cluster and decrease the effective charge of the cluster: both processes should decrease protonation behavior of the cluster. In the TMAOH solutions discussed above in which this oligomerization process is not so extensive, the pH is consistently greater than 13. These data strongly suggests that protonation is a key step to the oligomerization process: this is not surprising since protonation increases the lability of cluster oxo-ligands,<sup>56–58</sup> and can result in linkage of clusters via dehydration



The very different oligomerization behavior of **Rb1** and **Cs1** is intriguing, and evidence suggests that it is the greater ability of  $\text{Cs}^+$  to undergo contact ion-pairing that is inhibiting oligomerization by linkage through protonation and dehydration processes. It is interesting to recall that we have obtained these linked Keggin-ion materials with  $\text{Na}^+$  and  $\text{K}^+$  counterions only (not  $\text{Rb}^+$  or  $\text{Cs}^+$ ), which is consistent with the above analysis. However, the extensive chain-oligomerization of **Rb1** was somewhat surprising in that the monomeric clusters should be biccapped in a *trans* fashion to permit chain propagation. With only one cap per monomer cluster, we might expect only dimers. Three reasonable explanations include (1) the links between Keggin ions alternate between  $\text{A}^+$  ( $\text{A} = \text{alkali}$ ) and  $[\text{Nb}_2\text{O}_2]^{6+}$  (dimerized cap): both linkage types are observed in previously reported Keggin sheets,  $\text{K}_{10-x}[\text{Nb}_2\text{O}_2][\text{H}_x\text{GeNb}_{12}\text{O}_{40}] \cdot 11\text{H}_2\text{O}$ ;<sup>33</sup> (2) the caps are labile; and (3) linkage occurs from core-to-core or cap-to-core, in addition to cap-to-cap joining. Fitting the  $p(r)$  curve for 24 mmolar **Rb1** with six individual peaks (for the monomer, dimer, trimer, etc.) provided more detail for the linkage process; see Figure 5. The peaks for the long axes of the dimer, tetramer, and hexamer chains clearly have greater integrated peak area than for the trimer and pentamer chains. This suggests that (1) dimerization of the cap is the most favored; then (2) linkage of the dimers, either via a bridging Rb or core-to-core linkage, is favored over monomer–dimer linkage. The greater reactivity of the dimers is most likely directly related to size. We would expect a dimer to have less Brownian motion in solution than a monomer, and also perhaps a smaller hydration sphere. Therefore, it is likely easier for two larger particles to associate in close proximity so that linkage can occur.

Inset in Figure 5 is a plot of peak maxima from the PDDF Gaussian fit vs number of Keggin ions in the chain. The result is a very linear plot, illustrating the regular nature of chain growth via addition of discrete Keggin units. The slope is 8.3 Å per Keggin ion, which agrees well with the cap-to-cap distance of 8.5 Å (across the diameter of the Keggin ion), as estimated from the Keggin-layer structure shown in Figure 1D.<sup>33</sup> The cap-to-alkali distance is estimated to be approximately one angstrom larger; this lends support for a cap-to-core (monomer to dimer) or core-to-core (dimer to dimer) linking mechanism for formation of chains longer than the dimer.

Analysis of the PDDF fits of **Cs1** in water gave further evidence for a cap-to-core or core-to-core linking mechanism to form longer chains. All concentrations contain a population of monomers plus dimers (see Figure 6, for example). Since Cs would be more likely to bridge two dimers than Rb, we would expect **Cs1** in water to be more extensively oligomerized than **Rb1**, since the first step of dimerization does indeed occur. In

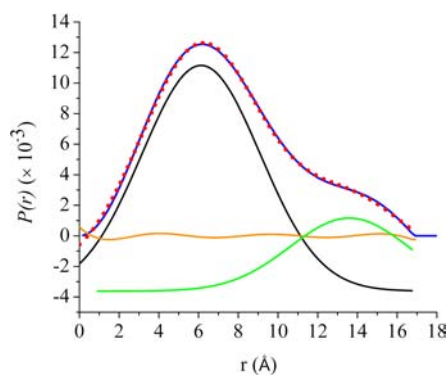


**Figure 6.** Fit of the PDDF analysis of 18 mM Cs1 in water. The black fitted peak is the monomer and the short axis of the dimer, and the green fitted peak is the long axis of the dimer. Yellow is the difference of the experiment (red dots) and the multi-peak Gaussian fit (blue line).

fact, it is probably extensive ion-association of Cs1 dimers with  $\text{Cs}^+$  that prevents further oligomerization via the core-to-core or cap-to-core bonding that is responsible for the longer chains of Rb1.

Figure 7 shows simulated PDDF for the capped monomer, dimer, and hexamer, using solX.<sup>59,60</sup> These were obtained by

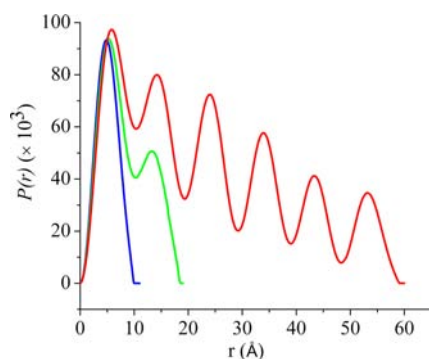


**Figure 7.** PDDF profiles for a capped monomer (blue), dimer (green), and hexamer (red), simulated using solX.<sup>59,60</sup>

calculating theoretical scattering curves from structures of the isolated monomer, dimer, and hexamer units (details in SI). The PDDF profiles were then generated in the same manner we obtain the experimental PDDF plots. By this qualitative treatment, we confirm that the solutions of Cs1 are always a mixture of monomers and dimers, and the solutions of Rb1 are a mixture of oligomeric forms.

As a final argument for protonation of the Nb=O cap being a key step to the cluster dimerization process, we present the structure (details available in SI) of Cs2 (*P*-1; CSD-426586),  $\text{Cs}_{18}\text{H}_6[(\text{NbOH})\text{SiNb}_{12}\text{O}_{40}]_2 \cdot 38\text{H}_2\text{O}$ ; see Figure 8. The crystal for this structure was isolated from an impure mixture, and thus was unfortunately not available for solution-based SAXS analysis. Nonetheless, we identified this dimer, along with 18 of 26 charge-balancing Cs-cations. The oxo-ligands bridging the capping Nb's have low bond valence sum values (1.17 and 1.25), indicating these two oxo ligands are protonated. Trans to the  $[\text{Nb}_2\text{O}_2]^{6+}$  bridging dimer on each cluster sits a  $\text{Cs}^+$  cation, bonded to four cluster oxo-ligands, in an identical manner to that observed in the Keggin sheets ( $\text{K}^+$  in Figure 1d).

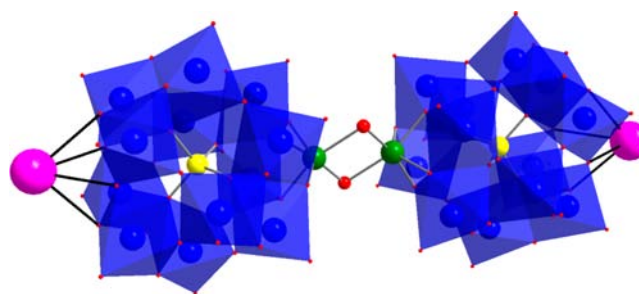


**Figure 8.** View of the capped dimer in Cs2. Green sphere is the bridging/capping Nb; red spheres are protonated bridging oxygen (protonation determined from BVS calculations); and pink spheres are two of the charge-balancing  $\text{Cs}^+$  cations (pink spheres), bonded in the same manner as the  $\text{K}^+$  in the layered structure shown in Figure 1d.

## CONCLUSIONS

In this study, we have isolated the monomeric and dimeric capped  $[(\text{NbO})\text{GeNb}_{12}\text{O}_{40}]^{13-}$  Keggin ions, the building blocks of previously reported framework materials of linked dodecaniobate Keggin ions. Under appropriate conditions, we can observe *in situ* oligomerization of clusters by X-ray scattering, and both cluster protonation and counterion-association play key roles in aqueous behavior of these clusters. This study illustrates the rich possibilities of probing solution behavior of metal-oxo clusters utilizing small-angle X-ray scattering, a technique that has been rarely used thus far for chemistry of discrete metal-oxo clusters such as polyoxometalates. Within the realm of aqueous metal-oxo cluster chemistry, Nb-POMs with their high solubility in maximum ion-association conditions uniquely provide opportunity for understanding solution-state phenomena including but not limited to self-assembly of materials and surface-coatings from soluble cluster building-blocks, crystallization and precipitation, electron transfer, and oxo ligand reactivity. These processes are universally important, yet poorly understood or controlled in aqueous systems in nature and in technology. Understanding aqueous phenomena of a well-constrained model such as Nb-POMs is the first step toward unveiling and controlling related processes that occur, without exception, in water in which cations and anions are present.

## ASSOCIATED CONTENT

### Supporting Information

Crystallographic Information files (cif) for Rb1 (CSD-426505), Cs1 (CSD-426588), and Cs2 (CSD-426586). PDF document containing experimental details on synthesis and data collection and analysis, data figures and tables for small-angle X-ray scattering, single crystal and powder X-ray diffraction, electrospray ionization mass spectrometry, thermogravimetry, and FTIR. This material is available free of charge via the Internet at <http://pubs.acs.org>.

## AUTHOR INFORMATION

### Corresponding Author

\*E-mail: [may.nyman@oregonstate.edu](mailto:may.nyman@oregonstate.edu).

### Present Address

Yu Hou, College of Chemistry, Chemical Engineering and Biotechnology, Donghua University, 2999 North Renmin Rd, Shanghai, 201620, China.

### Notes

The authors declare no competing financial interest.

## ACKNOWLEDGMENTS

This material is based upon work supported by the National Science Foundation under Grant No. CHE-1102637. Y.H. and M.N. acknowledge Sandia National Laboratories where they initiated the synthetic work. We thank Charles F. Campana (Bruker AXS Inc. Madison, WI) for assistance with the twin solution of Cs<sub>2</sub>. We are also very grateful for the assistance of Dr. Heiner Satner of Anton Parr GmbH (Graz Austria) in helping us become fluent in SAXS practice.

## REFERENCES

- (1) Limoges, B. R.; Stanis, R. J.; Turner, J. A.; Herring, A. M. *Electrochim. Acta* **2005**, *50*, 1169.
- (2) Lv, H. J.; Geletii, Y. V.; Zhao, C. C.; Vickers, J. W.; Zhu, G. B.; Luo, Z.; Song, J.; Lian, T. Q.; Musaev, D. G.; Hill, C. L. *Chem. Soc. Rev.* **2012**, *41*, 7572.
- (3) Mizuno, N.; Yamaguchi, K.; Kamata, K. *Coord. Chem. Rev.* **2005**, *249*, 1944.
- (4) Coronado, E.; Gomez-Garcia, C. J. *Chem. Rev.* **1998**, *98*, 273.
- (5) Khenkin, A. M.; Weiner, L.; Wang, Y.; Neumann, R. *J. Am. Chem. Soc.* **2001**, *123*, 8531.
- (6) Kim, W. B.; Voith, T.; Rodriguez-Rivera, G. J.; Dumesic, J. A. *Science* **2004**, *305*, 1280.
- (7) Kuo, M. C.; Stanis, R. J.; Ferrell, J. R.; Turner, J. A.; Herring, A. M. *Electrochim. Acta* **2007**, *52*, 2051.
- (8) Li, M. Q.; Shao, Z. G.; Scott, K. J. *Power Sources* **2008**, *183*, 69.
- (9) Rustad, J. R.; Casey, W. H. *Nat. Mater.* **2012**, *11*, 223.
- (10) Canioni, R.; Roch-Marchal, C.; Secheresse, F.; Horcajada, P.; Serre, C.; Hardi-Dan, M.; Ferey, G.; Greneche, J. M.; Lefebvre, F.; Chang, J. S.; Hwang, Y. K.; Lebedev, O.; Turner, S.; Van Tendeloo, G. *J. Mater. Chem.* **2011**, *21*, 1226.
- (11) Proust, A.; Matt, B.; Villanneau, R.; Guillemot, G.; Gouzerh, P.; Izzet, G. *Chem. Soc. Rev.* **2012**, *41*, 7605.
- (12) Song, J.; Luo, Z.; Britt, D. K.; Furukawa, H.; Yaghi, O. M.; Hardcastle, K. L.; Hill, C. L. *J. Am. Chem. Soc.* **2011**, *133*, 16839.
- (13) Song, Y. F.; Tsunashima, R. *Chem. Soc. Rev.* **2012**, *41*, 7384.
- (14) Nyman, M.; Rodriguez, M. A.; Shea-Rohwer, L. E.; Martin, J. E.; Proencio, P. P. *J. Am. Chem. Soc.* **2009**, *131*, 11652.
- (15) Nyman, M. D.; Desu, S. B.; Peng, C. H. *Chem. Mater.* **1993**, *5*, 1636.
- (16) Oliveri, A. F.; Carnes, M. E.; Baseman, M. M.; Richman, E. K.; Hutchison, J. E.; Johnson, D. W. *Angew. Chem., Int. Ed.* **2012**, *51*, 10992.
- (17) Judeinstein, P.; Livage, J. *J. Mater. Chem.* **1991**, *1*, 621.
- (18) Kaminski, R. C. K.; Pulcinelli, S. H.; Judeinstein, P.; Meneau, F.; Briois, V.; Santilli, C. V. *J. Phys. Chem. C* **2010**, *114*, 1416.
- (19) Gebauer, D.; Colfen, H. *Nano Today* **2011**, *6*, 564.
- (20) Knope, K. E.; Soderholm, L. *Chem. Rev.* **2013**, *113*, 944.
- (21) Michel, F. M.; Ehm, L.; Antao, S. M.; Lee, P. L.; Chupas, P. J.; Liu, G.; Strongin, D. R.; Schoonen, M. A. A.; Phillips, B. L.; Parise, J. B. *Science* **2007**, *316*, 1726.
- (22) Hu, Y. J.; Knope, K. E.; Skanthakumar, S.; Kanatzidis, M. G.; Mitchell, J. F.; Soderholm, L. *J. Am. Chem. Soc.* **2013**, *135*, 14240.
- (23) Gondikas, A. P.; Masion, A.; Auffan, M.; Lau, B. L. T.; Hsu-Kim, H. *Chem. Geol.* **2012**, *329*, 10.
- (24) Kellermeier, M.; Gebauer, D.; Melero-Garcia, E.; Drechsler, M.; Talmon, Y.; Kienle, L.; Colfen, H.; Garcia-Ruiz, J. M.; Kunz, W. *Adv. Funct. Mater.* **2012**, *22*, 4301.
- (25) Bajpe, S. R.; Breynaert, E.; Robeyns, K.; Houthoofd, K.; Absillis, G.; Mustafa, D.; Parac-Vogt, T. N.; Maes, A.; Martens, J. A.; Kirschhock, C. E. A. *Eur. J. Inorg. Chem.* **2012**, 3852.
- (26) Pigga, J. M.; Teprovich, J. A.; Flowers, R. A.; Antonio, M. R.; Liu, T. B. *Langmuir* **2010**, *26*, 9449.
- (27) Kojima, T.; Antonio, M. R.; Ozeki, T. *J. Am. Chem. Soc.* **2011**, *133*, 7248.
- (28) Bolze, J.; Peng, B.; Dingenouts, N.; Panine, P.; Narayanan, T.; Ballauff, M. *Langmuir* **2002**, *18*, 8364.
- (29) Qiu, J.; Nguyen, K.; Jouffret, L.; Szymanski, J. E. S.; Burns, P. C. *Inorg. Chem.* **2013**, *52*, 337.
- (30) Korala, L.; Brock, S. L. *J. Phys. Chem. C* **2012**, *116*, 17110.
- (31) Antonio, M. R.; Chiang, M. H.; Seifert, S.; Tiede, D. M.; Thiyagarajan, P. *J. Electroanal. Chem.* **2009**, *626*, 103.
- (32) Bonhomme, F.; Larentzos, J. P.; Alam, T. M.; Maginn, E. J.; Nyman, M. *Inorg. Chem.* **2005**, *44*, 1774.
- (33) Nyman, M.; Larentzos, J. P.; Maginn, E. J.; Welk, M. E.; Ingersoll, D.; Park, H.; Parise, J. B.; Bull, I.; Bonhomme, F. *Inorg. Chem.* **2007**, *46*, 2067.
- (34) Nyman, M.; Powers, C. R.; Bonhomme, F.; Alam, T. M.; Maginn, E. J.; Hobbs, D. T. *Chem. Mater.* **2008**, *20*, 2513.
- (35) Granadeiro, C. M.; de Castro, B.; Balula, S. S.; Cunha-Silva, L. *Polyhedron* **2013**, *52*, 10.
- (36) Mialane, P.; Lisnard, L.; Mallard, A.; Marrot, J.; Antic-Fidancev, E.; Aschehoug, P.; Vivien, D.; Secheresse, F. *Inorg. Chem.* **2003**, *42*, 2102.
- (37) Sadakane, M.; Dickman, M. H.; Pope, M. T. *Angew. Chem., Int. Ed.* **2000**, *39*, 2914.
- (38) Khan, M. I. *J. Solid State Chem.* **2000**, *152*, 105.
- (39) Zhang, Z. Y.; Lin, Q. P.; Kurunthu, D.; Wu, T.; Zuo, F.; Zheng, S. T.; Bardeen, C. J.; Bu, X. H.; Feng, P. Y. *J. Am. Chem. Soc.* **2011**, *133*, 6934.
- (40) Bu, W. M.; Ye, L.; Yang, G. Y.; Gao, J. S.; Fan, Y. G.; Shao, M. C.; Xu, J. Q. *Inorg. Chem. Commun.* **2001**, *4*, 1.
- (41) Duan, L. M.; Pan, C. L.; Xu, J. Q.; Cui, X. B.; Xie, F. T.; Wang, T. G. *Eur. J. Inorg. Chem.* **2003**, 2578.
- (42) Nyman, M.; Bonhomme, F.; Alam, T. M.; Rodriguez, M. A.; Cherry, B. R.; Krumhansl, J. L.; Nenoff, T. M.; Sattler, A. M. *Science* **2002**, *297*, 996.
- (43) Antonio, M. R.; Nyman, M.; Anderson, T. M. *Angew. Chem., Int. Ed.* **2009**, *48*, 6136.
- (44) Hou, Y.; Alam, T. M.; Rodriguez, M. A.; Nyman, M. *Chem. Commun.* **2012**, *48*, 6004.
- (45) Hou, Y.; Nyman, M.; Rodriguez, M. A. *Angew. Chem., Int. Ed.* **2011**, *50*, 12514.
- (46) Nyman, M. *Dalton Trans.* **2011**, *40*, 8049.
- (47) Nyman, M.; Burns, P. C. *Chem. Soc. Rev.* **2012**, *41*, 7354.
- (48) Nyman, M.; Celestian, A. J.; Parise, J. B.; Holland, G. P.; Alam, T. M. *Inorg. Chem.* **2006**, *45*, 1043.
- (49) Moore, P. B. *J. Appl. Crystallogr.* **1980**, *13*, 168.
- (50) Ilavsky, J.; Jemian, P. R. *J. Appl. Crystallogr.* **2009**, *42*, 347.
- (51) Son, J. H.; Ohlin, C. A.; Johnson, R. L.; Yu, P.; Casey, W. H. *Chem.—Eur. J.* **2013**, *19*, 5191.
- (52) Son, J. H.; Ohlin, C. A.; Larson, E. C.; Yu, P.; Casey, W. H. *Eur. J. Inorg. Chem.* **2013**, 1748.
- (53) Jehng, J. M.; Wachs, I. E. *Chem. Mater.* **1991**, *3*, 100.
- (54) Hardcastle, F. D.; Wachs, I. E. *Solid State Ionics* **1991**, *45*, 201.
- (55) Bridgeman, A. J. *Chem.—Eur. J.* **2006**, *12*, 2094.
- (56) Balogh, E.; Anderson, T. M.; Rustad, J. R.; Nyman, M.; Casey, W. H. *Inorg. Chem.* **2007**, *46*, 7032.
- (57) Black, J. R.; Nyman, M.; Casey, W. H. *J. Am. Chem. Soc.* **2006**, *128*, 14712.
- (58) Villa, E. M.; Ohlin, C. A.; Balogh, E.; Anderson, T. M.; Nyman, M. D.; Casey, W. H. *Angew. Chem., Int. Ed.* **2008**, *47*, 4844.
- (59) Tiede, D. M.; Zhang, R. T.; Chen, L. X.; Yu, L. H.; Lindsey, J. S. *J. Am. Chem. Soc.* **2004**, *126*, 14054.
- (60) Zhang, R. T.; Thiyagarajan, P.; Tiede, D. M. *J. Appl. Crystallogr.* **2000**, *33*, 565.